Decay of femtosecond laser-induced plasma filaments in air, nitrogen, and argon for atmospheric and subatmospheric pressures

N. L. Aleksandrov,[1] S. B. Bodrov,[2,3] M. V. Tsarev,[3] A. A. Murzanev,[2] Yu. A. Sergeev,[2] Yu. A. Malkov,[2] and A. N. Stepanov[2]

[1]*Moscow Institute of Physics and Technology, Dolgoprudny 141700, Russia*

[2]*Institute of Applied Physics, Russian Academy of Sciences, Nizhny Novgorod 603950, Russia*

[3]*University of Nizhny Novgorod, Nizhny Novgorod 603950, Russia*

(Received 19 April 2016; published 20 July 2016)

The temporal evolution of a plasma channel at the trail of a self-guided femtosecond laser pulse was studied experimentally and theoretically in air, nitrogen (with an admixture of ∼3% O_2), and argon in a wide range of gas pressures (from 2 to 760 Torr). Measurements by means of transverse optical interferometry and pulsed terahertz scattering techniques showed that plasma density in air and nitrogen at atmospheric pressure reduces by an order of magnitude within 3–4 ns and that the decay rate decreases with decreasing pressure. The argon plasma did not decay within several nanoseconds for pressures of 50–760 Torr. We extended our theoretical model previously applied for atmospheric pressure air plasma to explain the plasma decay in the gases under study and to show that allowance for plasma channel expansion affects plasma decay at low pressures.

DOI: 10.1103/PhysRevE.94.013204

I. INTRODUCTION

Different possible applications of light filaments including lightning protection [1,2], atmospheric remote sensing [3], microwave guiding [4,5], and terahertz generation [6–9] arouse interest in studying filamentation [10]. In some applications such as atmospheric remote sensing and microwave guiding, plasma filament time evolution is of primary importance. Several experimental techniques including electric conductivity measurement [11,12], optical transverse [11,13–15] and longitudinal [16] diffractometry, transverse terahertz scattering [17,18], and interferometry [17] were used to investigate plasma filament decay. Direct measurements with interferometry technique showed that, in air at atmospheric pressure, the peak plasma density reaches $\sim 10^{17}$ cm^{-3} for ∼1 m focusing and is then lowered by a factor of 5 within ∼300 ps [17]. Interferometry failed to measure plasma density on a longer (nanosecond) time scale, while the other techniques (terahertz scattering and cross conductivity) allowed tracing plasma density down to 10^{15} cm^{-3} for 2–3 ns [17,18].

Different kinetic models were proposed to explain the observed plasma filament decay in air. Simplified models described in several publications (see, for instance, [11,12,15]) considered basically several reactions including dissociative electron recombination with O_2^+ ions and three-body electron attachment to O_2 molecules with the rates that were usually assumed to be constant during the plasma decay and were adjusted to obtain agreement between calculated and measured plasma densities. A more comprehensive kinetic model developed in Refs. [17,18] showed an important role of dissociative electron-ion recombination with cluster ions ($O_2^+N_2$,O_4^+,$O_2^+H_2O$) and of three-body electron-ion recombination in the plasma filament decay, as well as the dependence of reaction rates on electron temperature that decreased during the plasma decay due to electron-impact excitation of molecules. Based on this model, agreement between calculations and measured data was reached.

Almost all studies of plasma filament decay were made in air at atmospheric pressure. For lower pressures, plasma filaments were investigated primarily in the initial phase of filament creation [19–22]. Plasma filament decay at low gas pressures was considered in Ref. [23] where the dynamics of plasma channel conductivity was measured on the microsecond time scale in air, nitrogen, and helium for the pressure range of 1.5–20 Torr.

It is more interesting for practical application to study plasma filament decay on pico- and nanosecond time scales when the plasma density is sufficiently high. In this work, using interferometry and terahertz scattering techniques, we consider plasma filament decay in air, nitrogen, and argon on the nanosecond time scale with picosecond resolution in a wide (2–760 Torr) pressure range. Using a numerical code that solves balance equations for the densities of gas species, their temperatures, and accounts for expansion of the plasma channel, we obtain good agreement with the experimental results and determine the dominant mechanisms of plasma recombination at low pressures.

II. EXPERIMENTAL SETUP

The scheme of the experiment is shown in Fig. 1. A Ti:sapphire laser system with 70-fs FWHM pulse duration and pulse energy up to 7 mJ was used to create and to probe plasma filament. Laser radiation was split into pump and probe pulses. The pump pulse with an energy of ∼4 mJ was focused by a 107 cm focal length spherical mirror in a chamber filled with different gases at various pressures p. We used air, nitrogen (with an admixture of $2.75 \pm 0.25\% O_2$), and argon. Plasma filament was formed near the focal plane and visualized by a CCD camera. We observed changes in the length and position of the filament with varying gas pressure (see the inset in Fig. 1). At atmosphere pressure, the filament was generated in air and nitrogen before the linear focus of the spherical mirror (at a distance of ∼100 cm from the mirror). When the pressure was decreased, the center of the filament shifted away from the focusing mirror toward the linear focus; this was explained by less profound Kerr self-focusing due to decreasing gas density [24]. The same effect led to a reduction of filament length from 5–7 cm at pressures 200–760 Torr

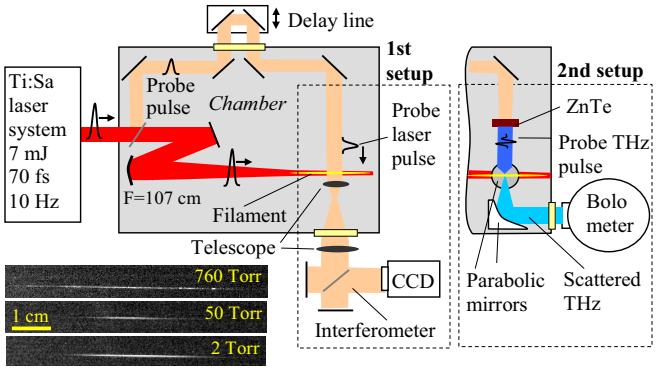

FIG. 1. Experimental setup. The inset shows the images of the filament at different pressures in air.

to ∼3 cm in the pressure range 20–100 Torr. At a lower pressure (2–10 Torr), the filament length increased again to ∼4−5 cm. The filament shortening at low pressures correlated with the decrease of the maximum electron concentration in the filament (see Fig. 4 below). Therefore, we expect that at 20–100 Torr a plasma-induced refraction will shorten the length of the plasma filament. However, the transition to lower pressures reduced the plasma density and, hence, the plasma refraction effect on laser radiation distribution near the linear focus. This led to the growth of the ionization region. In argon, the filament length was ∼3 cm independent of the gas pressure (at 50–760 Torr). In all cases, plasma density was measured near the filament center.

To study plasma density decay in the filament, we used the transverse optical interferometry and pulsed terahertz scattering techniques [17,18]. In optical interferometry, the probe femtosecond pulse, after passing a delay line, crossed the plasma filament perpendicularly, went into a Michelson interferometer with slightly tilted mirrors, and then formed an interferometric image on a CCD camera placed in one of the arms of the interferometer. An 8× telescope was placed in front of the interferometer to obtain better spatial resolution. The resulting plasma density distribution was numerically extracted from an interferometric image as described in Ref. [17]. The interferometry technique allowed us to measure plasma density in the filament down to $2-3\times10^{16}$ cm^{-3}. To measure lower plasma densities, the terahertz scattering technique was employed.

In the terahertz technique, the probe laser pulse (energy ∼0.5 mJ) generated a pulse of terahertz radiation (∼1−2 ps duration with central frequency near 1 THz) in a ZnTe crystal with appropriate time delay. The terahertz pulse was incident perpendicularly on the plasma filament (the pulse propagated normally to the drawing plate; Fig. 1) and focused by an off-axis parabola ($F = 5$ cm). Then, an identical parabola collected terahertz radiation scattered perpendicularly from the plasma (scattering direction is in the drawing plate; Fig. 1) and directed it into the input of a hot-electron He-cooled bolometer (QMS Instruments, model QFI/4). Efficient terahertz scattering was achieved because the transverse size of the plasma channel (∼150 μm) was comparable with the terahertz wavelength and the plasma density was close to the critical value corresponding to the terahertz frequency. Plasma density was obtained from the bolometer signal using a numerical code with the interferometric data for absolute calibration [17,18].

III. THEORETICAL DESCRIPTION AND COMPARISON WITH EXPERIMENT

A. Theoretical model

To simulate plasma filament decay at various pressures, we solved numerically a set of balance equations for charged and neutral particles simultaneously with the balance equation for electron temperature that affects the rate of electron loss. This simulation is similar to that made in our previous works [17,18] in which the filament decay in air at atmospheric pressure was studied. However, it was necessary to consider several additional effects that play an important role at reduced gas pressures while being negligible at the atmospheric pressure. At low pressures, the densities of charged particles in the filament are comparable with the densities of neutral species; therefore, temporal evolution of the densities of neutral particles must also be simulated. In addition, in this case, the energy released due to electron-ion recombination is distributed over a relatively small amount of neutral particles. This means that rapid gas heating in these reactions should be taken into account. Therefore, in our calculation, it is necessary to consider not only the balance equations for charged species and the equation for electron temperature, but the balance equation for neutral species and the equation for gas temperature as well.

At low gas pressures, plasma channel expansion can also lead to a decrease in the densities of plasma species. The velocity of the radial expansion of the plasma channel surrounded by a low-density medium depends on the specific deposited energy [25] and is of the same order of magnitude as the ion sound velocity [26]

$$C_s = \left(\frac{Z\gamma_e kT_e + \gamma_i kT_i}{m_i}\right)^{1/2}, \tag{1}$$

where $Z = 1$ is the relative ion charge, k is the Boltzmann constant, T_e and T_i are the electron and ion temperatures, respectively, m_i is the ion mass, and γ_e and γ_i are the specific heat ratios of the electron and ion gases, respectively. We take $\gamma_i = 7/5$ since most ions are diatomic and $\gamma_e = 1$ as the electrons in ion acoustic waves are isothermal [26, p. 146]. In our case, we supposed T_i to be equal to the gas temperature T. At atmospheric pressure, calculations predict electron temperature T_e in the 0.1–0.3 eV range on the nanosecond time scale (see Fig. 5 and [18]), while the ions remain at room temperature ($T_i \sim 0.03$ eV); in this case, from (1) we obtain $C_s \sim 1$ μm/ns. Thus, the radial expansion can be neglected for the first ten nanoseconds, if the initial radius of the plasma channel is around 60 μm [17]. At low (<50 Torr) pressures, electron thermalization in collisions with neutral particles is slower, whereas the ion temperature increases due to energy release in electron-ion recombination. As a result, the velocity of radial channel expansion increases by several times. In addition, at low pressures the interferometric measurements showed a decrease of the initial plasma channel radius down to ∼40 μm. Therefore, an increase in the plasma channel radius during the first five nanoseconds turns out to be comparable

with the initial radius. This means that channel expansion should be considered in plasma density calculation.

Assuming uniform densities of all plasma components in a cylindrically shaped filament and implying C_s to be the velocity of the filament boundary, the rate of density decrease can be written as

$$\left(\frac{dn}{dt}\right)_{\text{expan}} = -\frac{2C_s}{r}n, \tag{2}$$

where n is the density of a given charged or neutral specie,

$$r(t) = r_0 + \int_0^t C_s(t')dt' \tag{3}$$

is the radius of the plasma channel at an instant t, and r_0 is the initial radius of the channel, which was taken from the interferometric measurements. We used Eqs. (1), (2), and (3) to simulate the effect of plasma channel expansion on the densities of charged and neutral species when solving the corresponding balance equations.

In our case, the dominant mechanisms of plasma decay are electron dissociative recombination and three-body (the third body is an electron) recombination with simple ions generated by the laser pulse and with cluster ions formed due to ion conversion in the plasma channel. The balance equations for electrons and positive ions are expressed as

$$\frac{dn_e}{dt} = -n_e^2 \sum_j k_{3j}(T_e)n_{pj} - n_e \sum_j k_{2j}(T_e)n_{pj} + \left(\frac{dn_e}{dt}\right)_{\text{expan}} \tag{4}$$

and

$$\frac{dn_{pj}}{dt} = Q_{pj} - R_{pj} + \left(\frac{dn_{pj}}{dt}\right)_{\text{expan}}, \tag{5}$$

respectively. Here, n_e is the electron density, n_{pj} is the density of positive ions of the jth species, k_{3j} and k_{2j} are, respectively, the rate coefficients for three-body and two-body dissociative recombination of ions of the jth species, and Q_{pj} and R_{pj} are the terms describing formation and loss of these ions.

The balance equations for the densities of neutral particles (N_2, O_2, N, O, and Ar) are written by analogy with Eq. (5):

$$\frac{dN_j}{dt} = Q_j - R_j + \left(\frac{dN_j}{dt}\right)_{\text{expan}}. \tag{6}$$

Here, N_j is the density of neutral species of the jth species, and Q_j and R_j are, respectively, the terms describing formation and loss of these species.

The plasma was assumed to be uniform and the simulation was zero dimensional. The loss of charged particles due to ambipolar diffusion was neglected. Even for low pressures, this effect becomes important only for $t > 100$ ns, a time that is much longer than the characteristic time of plasma decay in this experiment. Electron attachment to oxygen molecules is also negligible for such short time intervals and this mechanism of electron loss was neglected.

Table I shows the reactions considered in the model and their rate coefficients. The model is based on that used previously [17,18] to simulate the plasma filament decay in atmospheric air. To describe plasma decay in N_2 and Ar, the model was extended to include electron recombination with N_2 and Ar ions and formation of cluster ions in these gases. In ambient air, the mole fraction of water vapor can be around 1%. Therefore, by analogy with our previous kinetic model of plasma decay in air at atmospheric pressure [18], we considered the formation of $O_2^+H_2O$ cluster ions and their recombination with electrons for air with H_2O at 20% relative humidity.

Electron temperature measurements for a plasma filament have not yet been done. Apparently, the difficulties for spectroscopic diagnostics arise from a low level of plasma luminosity and extremely fast (pico- and subnanosecond) time scales of plasma dynamics. The same is true for ion temperatures. Therefore, in the present work we rely on

TABLE I. Reactions and rates of electron-ion recombination and ion conversion.

No.	Reaction	Rate coefficient
1	$e^- + O_2^+ \rightarrow O + O$	$1.95 \times 10^{-7}\,(300/T_e)^{0.7}$ cm^3/s [27,28]
2	$e^- + e^- + M^+ \rightarrow e^- + M$ $M = O_2, N, N_2, Ar, Ar_2$	$2 \times 10^{-19}\,(300/T_e)^{9/2}$ cm^6/s [18]
3	$e^- + N_2O_2^+ \rightarrow N_2 + O_2$	$1.3 \times 10^{-6}\,(300/T_e)^{1/2}$ cm^3/s [29]
4	$e^- + O_4^+ \rightarrow O_2 + O_2$	$4.2 \times 10^{-6}\,(300/T_e)^{1/2}$ cm^3/s [28]
5	$e^- + H_2O \cdot O_2^+ \rightarrow O_2 + H_2O$	$2 \times 10^{-6}\,(300/T_e)^{1/2}$ cm^3/s [30]
6	$O_2^+ + 2N_2 \rightarrow N_2O_2^+ + O_2$	$0.9 \times 10^{-30}\,(300/T)^2$ cm^6/s [29]
7	$N_2O_2^+ + N_2 \rightarrow 2N_2 + O_2^+$	$1.1 \times 10^{-6}\,(300/T)^{5.3}\,e^{-2357/T}$ cm^3/s [29]
8	$O_2^+ + 2O_2 \rightarrow O_4^+ + O_2$	$2.4 \times 10^{-30}\,(300/T)^{3.2}$ [29]
9	$O_4^+ + O_2 \rightarrow O_2^+ + 2O_2$	$3.3 \times 10^{-6}\,(300/T)^4\,e^{-5030/T}$ cm^3/s [29]
10	$N_2O_2^+ + O_2 \rightarrow O_4^+ + N_2$	10^{-9} cm^3/s [29]
11	$H_2O + O_2^+ + M \rightarrow H_2O \cdot O_2^+ + M$ $M = O_2, N_2$	0.6×10^{-28} cm^6/s [30]
12	$N_2^+ + e^- \rightarrow N + N$	$1.8 \times 10^{-7}\,(300/T_e)^{0.39}$ cm^3/s [28]
13	$N_4^+ + e^- \rightarrow N_2 + N_2$	$1.4 \times 10^{-6}\,(300/T_e)^{0.41}$ cm^3/s [28]
14	$N_2^+ + N_2 + N_2 \rightarrow N_4^+ + N_2$	5×10^{-29} cm^3/s [29]
15	$e^- + Ar_2^+ \rightarrow e^- + 2\,Ar$	$9.1 \times 10^{-7}\,(300/T_e)^{0.61}$ cm^3/s [28]
16	$Ar^+ + 2\,Ar \rightarrow Ar_2^+ + Ar$	2.2×10^{-31} cm^6/s [31]

numerical calculations of the ion and electron temperatures evolution. The balance equation for electron temperature is written in the form

$$\frac{dT_e}{dt} = -(T_e - T)\nu_\varepsilon(T_e) - \frac{2}{3}T_e^2 n_e \sum_j \frac{dk_{3j}}{dT_e} n_{pj} - \frac{2}{3}T_e^2 \sum_j \frac{dk_{2j}}{dT_e} n_{pj}, \quad (7)$$

where $\nu_\varepsilon(T_e)$ is the frequency of electron energy relaxation in collisions with other particles. The last two terms on the right-hand side of (7) describe the effect of the so-called "recombination heating" [30]. This heating is due to the predominant recombination of low-energy electrons that leads to an increase in T_e. The frequency ν_ε for air, N_2, and Ar was taken from [32]. The initial value of electron temperature T_e $(t = 0)$ was assumed to be equal to 3 eV, a typical value of T_e in the filament plasma [33]. The calculated results are almost independent of $T_e(t = 0)$, because the frequency ν_ε decreases drastically with decreasing electron energy and the electrons rapidly "forget" their initial energy during the plasma decay.

Gas heating due to energy release in electron-ion recombination is described by the energy conservation equation

$$\frac{3N}{2}\frac{dT}{dt} = n_e \sum_j \Delta_{3j} k_{3j} n_{pj} + \sum_j \Delta_{2j} k_{2j} n_{pj}, \quad (8)$$

where Δ_{2j} and Δ_{3j} are, respectively, the energies released and transferred to gas heating in dissociative and three-body electron recombination of positive ions of the jth species. The values of Δ_{2j} were calculated on the basis of the measured branching ratios [28] for electron-ion dissociative recombination. Branching ratios for three-body recombination are unknown. As a zero approximation, we assumed that $\Delta_{3j} = \Delta_{2j}$. It is worth noting that, on the right-hand side of (8), the second term is much larger than the first one in our case and this approximation does not noticeably affect the calculated results.

B. Results and discussion

The measured and calculated temporal evolution of the plasma density for different gases and pressures is shown in Figs. 2–4. In argon [see Fig. 2(a)], we did not observe plasma density decay for 2 ns for all pressures studied. Here, only the interferometric technique was used to measure plasma density. On the other hand, the plasma filament decay in air and nitrogen was clearly observed in the time interval from 0 to 8 ns for the pressures studied [see Figs. 2(b)–2(d) and 3]. In both gases, the initial electron density in the plasma filament reached 10^{17}cm^{-3} for atmospheric pressure and was almost independent of the pressure in the 100–760 Torr range (Fig. 4). For lower pressures, the initial electron density decreased with decreasing pressure. The lower the gas pressure, the slower the plasma decay was. In particular, the electron density in air and nitrogen decreased by two orders of magnitude over the first seven nanoseconds at high pressures (500–760 Torr), while the density decreased only by an order of magnitude for the same period of time when the pressure was 2 Torr (Fig. 4).

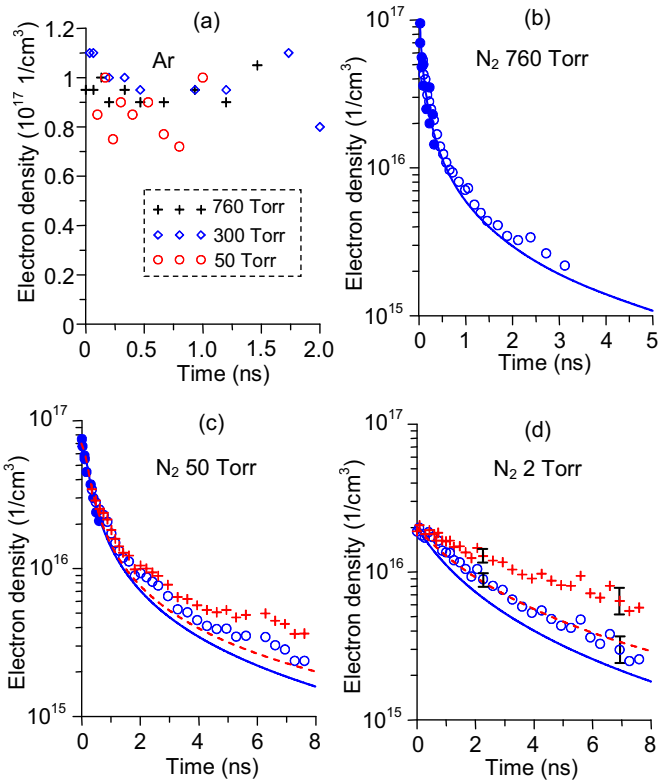

FIG. 2. Temporal evolution of electron density (a) in Ar and [(b)–(d)] in N_2 for various gas pressures. Symbols in (a) and closed circles in (b)–(d) correspond to interferometric measurements; the other symbols correspond to terahertz measurements and curves correspond to calculations. Calculations and terahertz measurements were made with considering [solid curves and open circles in (b)–d)] and neglecting [dashed curves and crosses in (c) and (d)] channel expansion. Vertical black straight lines in (d) are error bars for terahertz measurement data. The error of interferometric measurements may be estimated to be about 20% of experimental data statistics in (a).

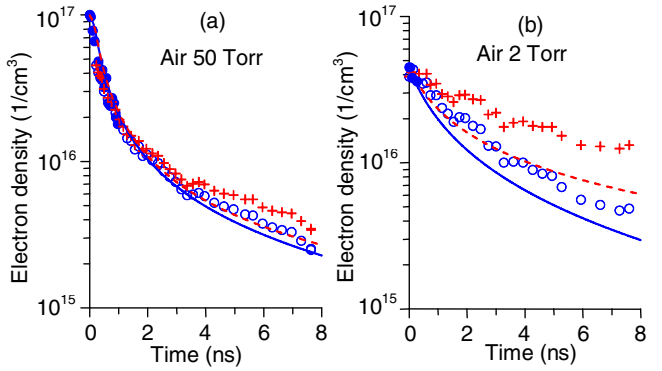

FIG. 3. Temporal evolution of electron density in air for (a) 50 and (b) 2 Torr. Closed circles correspond to interferometric measurements; the other symbols correspond to terahertz measurements and curves correspond to calculations. Calculations and terahertz measurements were made with considering (solid curves and open circles) and neglecting (dashed curves and crosses) channel expansion.

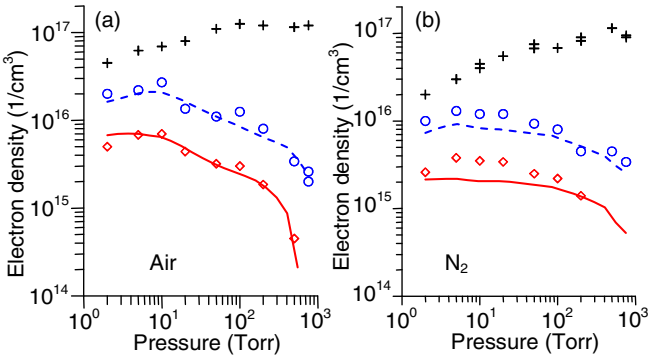

FIG. 4. Plasma density at $t = 0$ (crosses), 2 (circles), and 7 ns (diamonds) as a function of pressure for (a) air and (b) nitrogen ($t = 0$ corresponds to time of filament creation). Symbols correspond to experimental measurements. Dashed and solid curves correspond to calculations for 2 and 7 ns, respectively. The data are obtained with allowance for plasma expansion.

It is worth noting that, to measure plasma density by the terahertz scattering technique, the value of the plasma filament diameter must be known. This diameter was taken from interferometry measurements and in our previous consideration for air at atmospheric pressure was assumed to be constant during the filament decay [17,18]. At low pressures, this assumption is not correct and plasma filament expansion should be taken into account. In this work, we obtained the initial plasma diameter from interferometric data and calculated its temporal evolution using Eq. (3). The electron densities measured with the terahertz technique when considering or neglecting plasma channel expansion are compared in Figs. 2(c) and 2(d) for nitrogen and in Figs. 3(a) and 3(b) for air. In both cases, the effect of channel expansion leads to a decrease in the measured electron density by a factor of 2 for 2 Torr, whereas this decrease is much smaller for 50 Torr and negligible for atmospheric pressure.

There is no need to numerically simulate the plasma decay in Ar for explaining the fact that the electron density in Ar does not change in time for $\tau = 2$ ns [see Fig. 2(a)]. Let us consider plasma decay in this case for 760 Torr, $n_e(t = 0) = 10^{17}$ cm^{-3} and $T_e(t = 0) \sim 1$ eV. From the calculations [32] we have the electron energy relaxation frequency $\nu_\varepsilon(T_e = 1\ \text{eV}) \sim 3 \times 10^7\ \text{s}^{-1}$ in Ar under standard conditions. The effect of "recombination heating" can lead only to a slower electron energy relaxation and hence to lower recombination rates; we neglect this effect in our estimates for plasma decay in Ar. Thus, the characteristic time of the electron energy relaxation will be $\tau_\varepsilon = \nu_\varepsilon{}^{-1} \sim 30$ ns, much longer than τ; that is, the electrons have no time to thermalize and T_e does not change for 2 ns. In the Ar plasma, the electron loss is controlled by three-body recombination with Ar^+ and $Ar_2{}^+$ ions [reaction 2 in Table I] and by dissociative recombination with $Ar_2{}^+$ ions (reaction 15). Primary ions generated in the filament are Ar^+ and $Ar_2{}^+$; they are formed via three-body reaction 16. The characteristic time of this process is $\tau_{16} = (k_{16}N^2)^{-1} \sim 8$ ns, where N is the gas density. We have $\tau_{16} > \tau$ and Ar^+ ions are the dominant ion species in our case. The characteristic time of reaction 2 is $\tau_2 = [k_2(T_e = 1\ \text{eV})n_e{}^2(t = 0)]^{-1} \sim 14$ ns, much longer than the time of observation τ. Therefore, the electron density in the Ar plasma does not change in time for 760 Torr. It is expected that the same is also true for reduced gas pressures because the rate of three-body formation of $Ar_2{}^+$ ions and the rate of electron energy relaxation decrease with decreasing pressure.

Plasma decay in air and N_2 was simulated on the basis of numerical solution of Eqs. (1)–(8). In our experiment, nitrogen with a small (2.75%) addition of O_2 was used. For typical laser intensities in the filament [10], the ionization frequency of O_2 in the plasma filament is around three orders of magnitude higher that the ionization frequency of N_2. Therefore, in our calculations we assumed that oxygen is first ionized and the remaining electron and ion densities are due to nitrogen ionization.

Figures 2(b), 2(c), 3, and 4 compare the calculated and measured evolutions of the electron density in N_2 and air for various gas pressures. Our calculations show a decrease in the rate of plasma decay with decreasing gas pressure in N_2 and air. There is a good agreement between calculations and measurements in atmospheric pressure N_2 (even when plasma channel expansion is neglected). The same was obtained for the plasma decay in air at atmospheric pressure (see [17]). However, the lower the gas pressure, the larger the difference between the calculated and measured electron densities. According to our calculations, the loss of charged particles in nitrogen and air at low pressures is controlled by dissociative electron recombination with simple $N_2{}^+$ and $O_2{}^+$ ions. These reactions have been thoroughly studied and their rate coefficients are well known [28]. Therefore, the obtained difference between calculated and measured electron densities for low pressures cannot be explained by the uncertainty in the recombination coefficients. Figures 2–4 show that, taking into account plasma channel expansion, it is possible to reach a better agreement between calculated and measured data for air and nitrogen even at low gas pressures. It should be noted that we have crudely considered the effect of channel expansion on the plasma decay for low pressures. To simulate this effect consistently, it is necessary to solve the equations at least in the one-dimensional approximation. During plasma channel expansion, the thermal energy of charged particles is converted to the energy of their collective motion. Light electrons and heavy ions move with different velocities. As a result, an ambipolar electric field is created due to charge separation. The evolution of this field should be simulated consistently with the simulation of plasma channel expansion during plasma decay. The velocity distributions of charged particles become anisotropic and a kinetic approach is required to simulate channel expansion and radial distribution of plasma parameters adequately. This consideration is beyond the scope of our work. It is worth noting that, for a sufficiently high energy input, the radial velocity of plasma channel expansion is mainly governed by the specific deposited energy and is almost independent of other parameters [25]. Therefore, our treatment of channel expansion should be considered as a reasonable approximation when there is no need to determine radial distributions of plasma parameters.

Reasonable agreement between calculations and measurements was obtained at low pressures only when considering the fact that in this case electron energy relaxation is slow and gas heating is important. Figures 5 and 6 show, respectively,

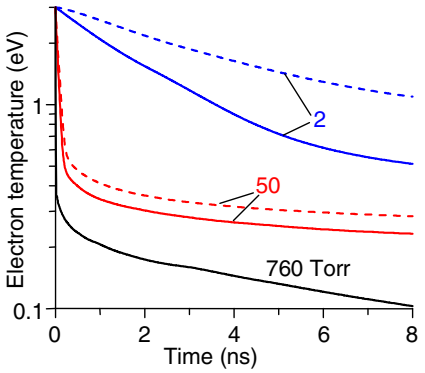

FIG. 5. Theoretically calculated temporal evolution of electron temperature in N_2 (solid lines) and air (dashed lines) for various gas pressures.

the calculated temporal evolution of electron temperature T_e and gas temperature T in N_2 and in air for various gas pressures. Here, the lower the gas pressure, the higher T_e and T are. The increase in T is due to the energy release in electron-ion recombination that is distributed over a smaller amount of particles at low gas pressures. The increase in T_e with decreasing gas pressure is explained (i) by a decrease in the rate of electron temperature relaxation due to the lower frequency ν_ε and (ii) due to the higher values of T to which T_e tends during relaxation.

Figures 7 and 8 show the temporal evolution of the electron loss frequencies for different channels of electron loss in N_2 and air, respectively. At high pressures, there are several channels of electron loss; they are three-body electron-ion recombination and dissociative recombination with simple molecular and cluster ions. At low pressures, the mechanisms of electron loss are much simpler. Here, the loss of electrons is dominated by dissociative electron recombination with simple N_2^+ and O_2^+ ions; the rates of these reactions decrease with increasing electron temperature. This is the main reason for a lower rate of plasma decay at lower gas pressures. In addition, in this case recombination of cluster ions is not important because they are formed in three-body reactions that are not efficient for low pressures. Finally, three-body electron-ion recombination is negligible at low pressures because its rate

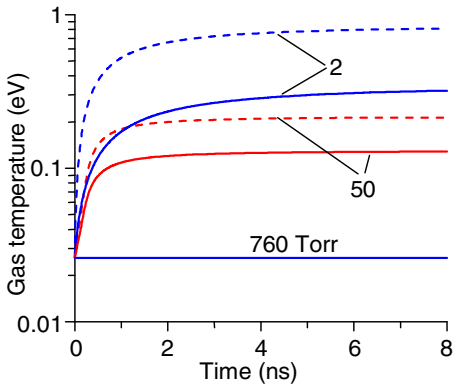

FIG. 6. Theoretically calculated temporal evolution of gas temperature in N_2 (solid lines) and air (dashed lines) for various gas pressures.

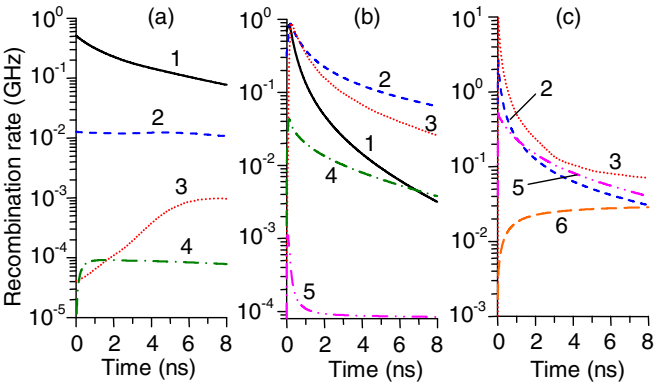

FIG. 7. Theoretically calculated temporal evolution of electron loss frequencies for different channels of electron loss in N_2 for (a) 2, (b) 50, and (c) 760 Torr: dissociative recombination with N_2^+ (1), dissociative recombination with O_2^+ (2), three-body recombination (3), dissociative recombination with N_4^+ (4), dissociative recombination with $N_2O_2^+$ (5), and dissociative recombination with O_4^+ (6).

decreases drastically with increasing electron temperature that is higher for low pressures (see Fig. 7).

IV. CONCLUSIONS

We have studied experimentally and numerically plasma filament decay in air, nitrogen (with a small admixture of O_2), and argon in the gas pressure range from 2 to 760 Torr. Time-resolved electron density measurements by the transverse optical interferometry and pulsed terahertz scattering techniques showed that the rate of plasma decay in air and nitrogen decreases with decreasing gas pressure. In air and nitrogen at atmospheric pressure, the plasma density decreased by two orders of magnitude in 3–4 ns, whereas only an order of magnitude decrease in the plasma density was observed in those gases in 8 ns when the gas pressure was reduced to 2–5 Torr. There was no sign of plasma decay in Ar for 2 ns, although the pressure was varied from 50 to 760 Torr.

A computational kinetic model was developed to simulate plasma filament decay for reduced gas pressures in air, N_2,

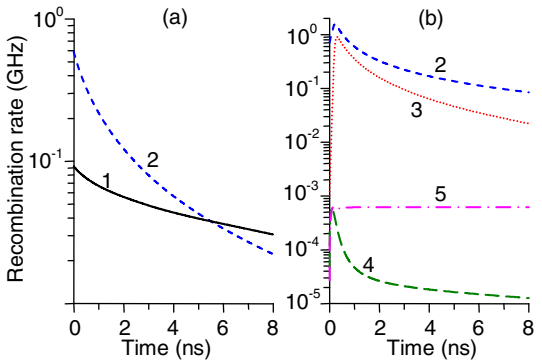

FIG. 8. Theoretically calculated temporal evolution of electron loss frequencies for different channels of electron loss in air for (a) 2 and (b) 50 Torr: dissociative recombination with N_2^+ (1), dissociative recombination with O_2^+ (2), three-body recombination (3), dissociative recombination with $N_2O_2^+$ (4), and dissociative recombination with $H_2O \cdot O_2^+$ (5).

and Ar. In contrast to the case of atmospheric pressure plasma decay, this model took into account a decrease in the density of neutral particles and gas heating due to energy release in electron-ion recombination (the latter effect was studied earlier in [17] but turned out to be negligible at atmospheric pressures). It was shown that the atmospheric pressure Ar plasma did not decay for several nanoseconds because the initial electron temperature was high, whereas electron energy relaxation was slow. As a result, the rate of three-body electron recombination with Ar^+ ions was too low to cause plasma decay. In addition, $Ar_2{}^+$ ions that could efficiently recombine with electrons had no time to be formed and to favor plasma decay for the period of time under study.

Our simulation of the plasma filament decay in air and N_2 showed that the observed decrease in the decay rate with decreasing gas pressure is explained by higher values of electron temperature in comparison with the case of atmospheric pressure. Indeed, the gas temperature in the decaying plasma filament is elevated for low gas pressures owing to energy release in electron-ion recombination. This and a decrease in the rate of electron energy relaxation led to an increase in the electron temperature with decreasing gas pressure and consequently to a decrease in the rate of electron-ion recombination. In addition, the formation of cluster ions that are characterized by high recombination rates was not important for low gas pressures.

There was good agreement between calculated and measured electron density histories in atmospheric pressure air and N_2, whereas the difference between the calculated and measured results increased when the gas pressure decreased. Our calculations showed that this could be associated with the effect of plasma channel expansion that is negligible at atmospheric pressure and becomes important for low pressures.

The obtained results can be used for application of laser filaments to remote sensing of gases at low pressures.

ACKNOWLEDGMENTS

This work was supported in part by the Russian Ministry of Education and Science (state Contract No. 14.Z50.31.0007) and the Russian Foundation for Basic Research (Grant No. 15-32-21049). S.B.B. and M.V.T. acknowledge support from the Russian Ministry of Education and Science under Agreement No. 02.B.49.21.0003 with the University of Nizhny Novgorod.

[1] M. Rodriguez, R. Sauerbrey, H. Wille, L. Woste, T. Fujii, Y.-B. Andre, A. Mysyrowicz, L. Klingbeil, K. Rethmeier, W. Kalkner, J. Kasparian, E. Salmon, J. Yu, and J.-P. Wolf, Opt. Lett. **27**, 772 (2002).

[2] S. B. Leonov, A. A. Firsov, M. A. Shurupov, J. B. Michae, M. N. Shneider, R. B. Miles, and N. A. Popov, Phys. Plasmas **19**, 123502 (2012).

[3] J. Kasparian, M. Rodriguez, G. Mejean, J. Yu, E. Salmon, H. Wille, R. Bourayou, S. Frey, Y.-B. Andre, A. Mysyrowicz, R. Sauerbrey, J.-P. Wolf, and L. Woste, Science **301**, 61 (2003).

[4] M. Châteauneuf, S. Payeur, J. Dubois, and J.-C. Kieffer, Appl. Phys. Lett. **92**, 091104 (2008).

[5] M. N. Shneider, A. M. Zheltikov, and R. B. Miles, J. Appl. Phys. **108**, 033113 (2010).

[6] C. D'Amico, A. Houard, S. Akturk, Y. Liu, J. Le Bloas, M. Franco, B. Prade, A. Couairon, V. T. Tikhonchuk, and A. Mysyrowicz, New J. Phys. **10**, 013015 (2008).

[7] J.-F. Daigle, F. Théberge, M. Henriksson, T.-J. Wang, S. Yuan, M. Châteauneuf, J. Dubois, M. Piché, and S. L. Chin, Opt. Express **20**, 6825 (2012).

[8] L. Bergé, S. Skupin, C. Köhler, I. Babushkin, and J. Herrmann, Phys. Rev. Lett. **110**, 073901 (2013).

[9] T.-J. Wang, J.-F. Daigle, Y. Chen, C. Marceau, F. Théberge, M. Châteauneuf, J. Dubois, and S. L. Chin, Laser Phys. Lett. **7**, 517 (2010).

[10] A. Couairon and A. Mysyrowicz, Phys. Rep. **441**, 47 (2007).

[11] S. Tzortzakis, B. Prade, M. Franco, and A. Mysyrowicz, Opt. Commun. **181**, 123 (2000).

[12] J. Zhu, Z. Ji, Y. Deng, J. Liu, R. Li, and Z. Xu, Opt. Express **14**, 4915 (2006).

[13] G. Rodriguez, A. R. Valenzuela, B. Yellampalle, M. J. Schmitt, and K.-Y. Kim, J. Opt. Soc. Am. B **25**, 1988 (2008).

[14] Z. Sun, J. Chen, and W. Rudolph, Phys. Rev. E **83**, 046408 (2011).

[15] H. Yang, J. Zhang, Y. Li, J. Zhang, Y. Li, Z. Chen, H. Teng, Z. Wei, and Z. Sheng, Phys. Rev. E **66**, 016406 (2002).

[16] J. Liu, Z. Duan, Z. Zeng, X. Xie, Y. Deng, R. Li, Z. Xu, and S. L. Chin, Phys. Rev. E **72**, 026412 (2005).

[17] S. Bodrov, V. Bukin, M. Tsarev, A. Murzanev, S. Garnov, N. Aleksandrov, and A. Stepanov, Opt. Express **19**, 6829 (2011).

[18] S. Bodrov, N. Aleksandrov, M. Tsarev, A. Murzanev, I. Kochetov, and A. Stepanov, Phys. Rev. E **87**, 053101 (2013).

[19] G. Méchain, T. Olivier, M. Franco, A. Couairon, B. Prade, and A. Mysyrowicz, Opt. Commun. **261**, 322 (2006).

[20] A. Couairon, M. Franco, G. Méchain, T. Olivier, B. Prade, and A. Mysyrowicz, Opt. Commun. **259**, 265 (2006).

[21] S.-Y. Li, F.-M. Guo, Y. Song, A.-M. Chen, Y.-J. Yang, and M.-X. Jin, Phys. Rev. A **89**, 023809 (2014).

[22] S. Hosseini, O. Kosareva, N. Panov, V. P. Kandidov, A. Azarm, J.-F. Daigle, A. B. Savel'ev, T.-J. Wang, and S. L. Chin, Laser Phys. Lett. **9**, 868 (2012).

[23] N. Vujičić, H. Skenderović, T. Ban, D. Aumiler, and G. Pichler, Appl. Phys. B **82**, 377 (2006).

[24] Á. Börzsönyi, Z. Heiner, A. P. Kovács, M. P. Kalashnikov, and K. Osvay, Opt. Express **18**, 25847 (2010).

[25] D. S. Dorozhkina and V. E. Semenov, Phys. Rev. Lett. **81**, 2691 (1998).

[26] N. A. Krall and A. W. Trivelpiece, *Principles of Plasma Physics* (McGraw-Hill, New York, 1973).

[27] F. J. Mehr and M. A. Biondi, Phys. Rev. **181**, 264 (1969).

[28] A. I. Florescu-Mitchell and J. B. A. Mitchell, Phys. Rep. **430**, 277 (2006).

[29] I. A. Kossyi, A. Yu. Kostinsky, A. A. Matveyev, and V. P. Silakov, Plasma Sources Sci. Technol. **1**, 207 (1992).

[30] N. L. Aleksandrov, S. V. Kindysheva, M. M. Nudnova, and A. Yu. Starikovskiy, J. Phys. D: Appl. Phys. **43**, 255201 (2010).

[31] B. M. Smirnov, *Complex Ions* (Nauka, Moscow, 1983) (in Russian).

[32] E. M. Anokhin, M. A. Popov, I. V. Kochetov, N. L. Aleksandrov, and A. Yu. Starikovskii, Plasma Phys. Rep. **42**, 59 (2016).

[33] D. Kartashov, S. Alisauskas, A. Pugzlys, M. Shneider, and A. Baltuska, J. Phys. B: At., Mol. Opt. Phys. **48**, 094016 (2015).